International Journal of Pavement Engineering

ISSN: 1029-8436 (Print) 1477-268X (Online) Journal homepage: https://www.tandfonline.com/loi/gpav20

Performance assessment of Kinect as a sensor for pothole imaging and metrology

Khurram Kamal, Senthan Mathavan, Tayyab Zafar, Imran Moazzam, Ahsan Ali, S. Usman Ahmad & Mujib Rahman

To cite this article: Khurram Kamal, Senthan Mathavan, Tayyab Zafar, Imran Moazzam, Ahsan Ali, S. Usman Ahmad & Mujib Rahman (2018) Performance assessment of Kinect as a sensor for pothole imaging and metrology, International Journal of Pavement Engineering, 19:7, 565-576, DOI: 10.1080/10298436.2016.1187730

To link to this article: https://doi.org/10.1080/10298436.2016.1187730

Published online: 01 Jun 2016.

INTERNATIONAL JOURNAL OF PAVEMENT ENGINEERING, 2018
VOL. 19, NO. 7, 565–576
https://doi.org/10.1080/10298436.2016.1187730

Taylor & Francis
Taylor & Francis Group

Performance assessment of Kinect as a sensor for pothole imaging and metrology*

Khurram Kamal[a], Senthan Mathavan[b], Tayyab Zafar[a], Imran Moazzam[a], Ahsan Ali[a], S. Usman Ahmad[a] and Mujib Rahman[c]

[a]Department of Mechatronics Engineering, College of E&ME, National University of Sciences and Technology, PRISM Group, Islamabad, Pakistan; [b]School of Architecture, Design and the Built Environment, Nottingham Trent University, Nottingham, UK; [c]School of Engineering and Design, Brunel University, Uxbridge, UK

ABSTRACT

Potholes are one of the key defects that affect the performance of roads and highway networks. Metrological features of a pothole provide useful metrics for road distress measurement and severity analysis. This paper presents a performance analysis of Kinect as a sensor for pothole imaging and metrology. Depth images of paved surfaces are collected from concrete and asphalt roads using this sensor. Three-dimensional (3D) meshes are generated for a variety of pothole configurations in order to visualise and to calculate their different metrological features. The sensor is benchmarked using a test-rig with pothole-like depressions or artificial potholes of known dimensions to evaluate sensor performance under different real-life imaging conditions, such as through the media of clear, muddy and oily water. Error in measurement due to surface roughness is also studied. Another source of error that is due to the presence of foreign objects such as stones and pebbles in the form of negative depth, is also discussed and compensated. Results show that a mean percentage error of 2.58 and 5.47% in depth and volumetric calculations, respectively.

ARTICLE HISTORY
Received 20 October 2015
Accepted 5 May 2016

KEYWORDS
Automation; pavement maintenance; image processing; performance analysis; pothole metrology

1. Introduction

Potholes are a frequent occurrence in many parts of highway networks and are a source of irritation to drivers and a key concern for road maintenance authorities. These localised defected areas also reduce ride quality and potentially create a dangerous driving condition. It is reported that potholes are a main reason for axle and suspension failures in vehicles. This is the third most frequent mechanical damage that costs about £2.8 billion per annum to the British drivers. It is reported that concerned authorities in Britain pay more than 30 million pounds in compensation claims due to poor roads (Asphalt Industry Alliance 2014). The problem is also severe in the US, as New York City Department of Transportation has filled about 113,000 potholes in 2014 (Picche 2013). In this context, an accurate volumetric estimation of filler material for pothole repair over a particular run of road is of great importance for maintenance purposes. Specifically, the volume estimation helps to avoid any shortage or excess of filler material that is often transported to site from a different location, thus, reducing the wastage of material as well as the transportation cost. Geometrical and metrological information is also important to define the extent and severity of potholes. In addition to this, from an efficiency point of view, a manual survey of potholes is not only a slow process, it also cannot measure the volume of a pothole, let alone accurately. The manual assessment is subjective and it may be hazardous for road inspectors, from a safety perspective (Bianchini *et al.* 2010). Advancements in the field of image processing and machine-vision have added automation, removed the subjectivity element and improved the quality of road assessments when compared with manual surveys. A number of methods have been proposed for pothole detection and characterisation so far. In addition to manual measurements, vibration measurements, image and video analysis, stereo-vision, and laser based techniques are in common practice.

This paper is an extension of work that proposes the usage of Kinect as a sensor for metrology and visualisation of potholes (Moazzam *et al.* 2013). Depth images of paved surfaces were collected from concrete and asphalt roads. 3D meshes were generated for a variety of potholes in order to visualise and to calculate their different metrological features. The sensor was found to have a great potential for pavement imaging as it provides more detailed information of distress measurement and metrology of potholes as compared to simple vision techniques. Also, the approach is found better than stereo-vision approach in a sense as depth measured by Infrared (IR) camera is readily available and no extra computation is required. It is also cheaper as compared to lasers.

The main contribution of the research is to evaluate the performance of Kinect-based pavement assessment in static conditions. The research focuses on the benchmarking and performance measurement of Kinect against artificially created potholes of standard and known dimensions. The sensor is tested under different conditions such as pothole filled with clear

CONTACT Khurram Kamal k.kamal@ceme.nust.edu.pk
*This paper has not been published elsewhere and that it has not been submitted simultaneously for publication elsewhere.

water, muddy water and water mixed with oil. The research also provides study on effect of surface roughness on measurements made by the Kinect sensor. The algorithm is made more robust or reliable by benchmarking it against shapes of known dimensions using a more practical approach (Gonzalez-Jorge *et al.* 2013). Negative depth due to the presence of different objects such as leaves, stones and pebbles, near the potholes is addressed and its effects are compensated. These factors have not been addressed in the literature so far, while considering Kinect as a sensor for pothole imaging.

Section 2 of the paper briefly reviews the use of Kinect in pothole surveys. Next, Section 3 explains features of the Kinect sensor and its usage in pavement applications. The experimental set-up is described in Section 4, whereas Sections 5 and 6 detail out the algorithm and initial results, respectively. Finally, Section 7 explains benchmarking and performance analysis.

2. Pothole surveys: a technology review

Numerous techniques are reported in literature to detect and assess potholes. Eriksson *et al.* (2008) studied mobile sensing of roads to monitor and report potholes. Accelerometer and Global Positioning System (GPS) are used to detect and locate potholes, respectively. A major drawback of the technique is that it requires at least one of the tires moving over a pothole. A similar approach was proposed by Aksamit and Szmechta (2011) using built-in accelerometer and GPS of a smartphone. Many researchers have employed image- and vision-based techniques for exploring potholes. These techniques include stereo-vision, or use of a camera in combination with an optical device such as laser or Light Emitting Diode (LED). Koch and Brilakis (2011) studied vision tracking of potholes for road surveys. This approach proposes pothole detection using video sequences. In this approach, the texture of potholes is compared with a reference texture of pavement for detection. The approach proposes a kernel-based tracking of potholes. However, the proposed approach is based on digital imaging that does not provide depth data – a major disadvantage in assessing severity. Rajab *et al.* (2008) proposed a curve fitting-based technique for 2D pavement images in order to extract the geometrical and metrological features of potholes. Jog *et al.* (2012) proposed a vision-based technique for automatic detection and severity assessment of potholes. An image sequence is acquired from rear view camera of a car. A 2D intensity-based detection in combination with a 3D sparse reconstruction algorithm is used to confirm the existence of a pothole in the video sequence. The outcome of 3D sparse reconstruction algorithm is then fed to a dense reconstruction algorithm in order to generate a dense 3D point cloud model. Yao *et al.* (2008) used the second-order moment operator on pavement surface images and calculated major axis, minor axis and orientation of potholes. Also, other approaches based on support vector machines and genetic algorithms in order to extract pothole features have also been proposed (Jin and Yayu 2010, Salari and Yu 2011). All of these techniques rely on 2D imaging, thus lacking the accurate volume information.

Youquan *et al.* (2011) performed pothole detection using the principle of triangulation. A line LED and two cameras are used in this approach. Salari and Bao (2011) used stereo vision for pavement distress evaluation. Two cameras are used to take images of same scene. The cameras are kept apart by a small distance. From the two images taken, similar points are matched leading to 3D reconstruction. The technique has an advantage in that it is not affected by foreign objects such as shadows, oil spills and tire marks. Wang and Gong (2002) also proposed stereo-vision to calculate the depth of potholes. The major drawback with the stereo-vision-based techniques is high computational effort and high data storage requirement. Moreover, stereo-vision has surface reconstruction and correspondence problems that need to be addressed as well (Liu 2006). Laser-based techniques in combination with vision-based techniques have also been reported in the literature (Laurent *et al.* 1997, Yu and Salari 2011)

3. Pothole detection using Kinect sensor

Kinect sensor is a low-cost sensor that costs around \$100. It consists of an IR camera and an Red Green Blue (RGB) camera. The IR camera operates at 30 fps with image resolution of 640 × 480 pixels and with higher image resolution of 1280 × 1024 pixels at 10 fps. The angle of view is 58° horizontal, 45° vertical and 70° diagonal. The operating range is 0.8–3.5 m (Cruz *et al.* 2012). A tilt motor, an accelerometer, and microphones are built-in. Kinect provides two types of images, an RGB image and a depth image. The sensor has found its use in areas such as robotics and gaming (Rakprayoon *et al.* 2011, Correa *et al.*2012, El-laithy *et al.* 2012).

Table 1. Comparison of measurement techniques.

Techniques	Strengths	Limitations
Accelerometer	• Lowest data storage • Cost-effective	• Low accuracy • Many non-detections
Simple vision	• Pothole detection ability • Pothole span can be calculated	• No depth information • Incomplete detections • Effected by Shading, Oil Spills, etc.
Stereo vision	• Better accuracy • Depth can be calculated	• High computational effort • High data storage
Lasers	• Accurate depth measurements	• High initial costs • Significant power consumption • High maintenance cost
Kinect	• Less computational effort • Less storage • Low cost • Less power hungry	• Measurements affected by direct sunlight, metal surfaces, water, dirt, stones, etc.

Figure 1. Experimental setup.

Joubert *et al.* (2011) deployed a GPS, Kinect and a USB camera for pothole localisation and data collection. A GPS is used to locate the coordinates of potholes. A plane of the road surface is estimated using RANdom SAmple Consensus (RANSAC) method and then the depth image is subtracted from the estimated plane. Pothole width is calculated using Kinect images by manually selecting the two opposite points on the pothole contour. Edges of potholes are detected from camera video sequence. The system records 3D point cloud data and location of detected potholes; the data is analysed and processed to get the width and depth of a given pothole. The system is designed to perform surveys at vehicle speeds up to 60 km/h. However, it has a limitation that it provides a very basic information regarding pothole width and depth using Kinect.

Jahanshahi *et al.* (2012) employed Kinect sensor for pavement distress measurement. Depth images from sensor are used to detect defects in pavement. Again, RANSAC is used for plane fitting. The Otsu thresholding method is used to discriminate between defective and normal areas of road (Gonzalez and Woods 2004). Rectangles are fitted to detected defects in images in order to calculate length and width of pothole. A GPS is used to localise the defects on map. The algorithm validates results in

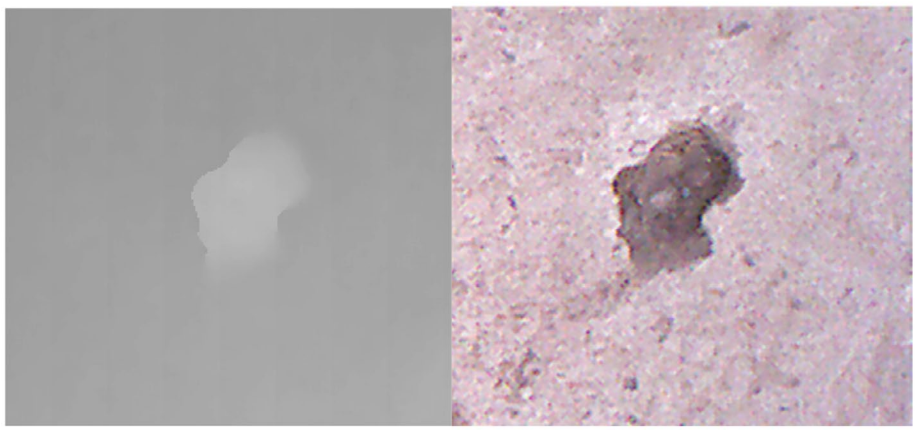

Figure 2. Depth image (left) and RGB image of pothole using Kinect (right).

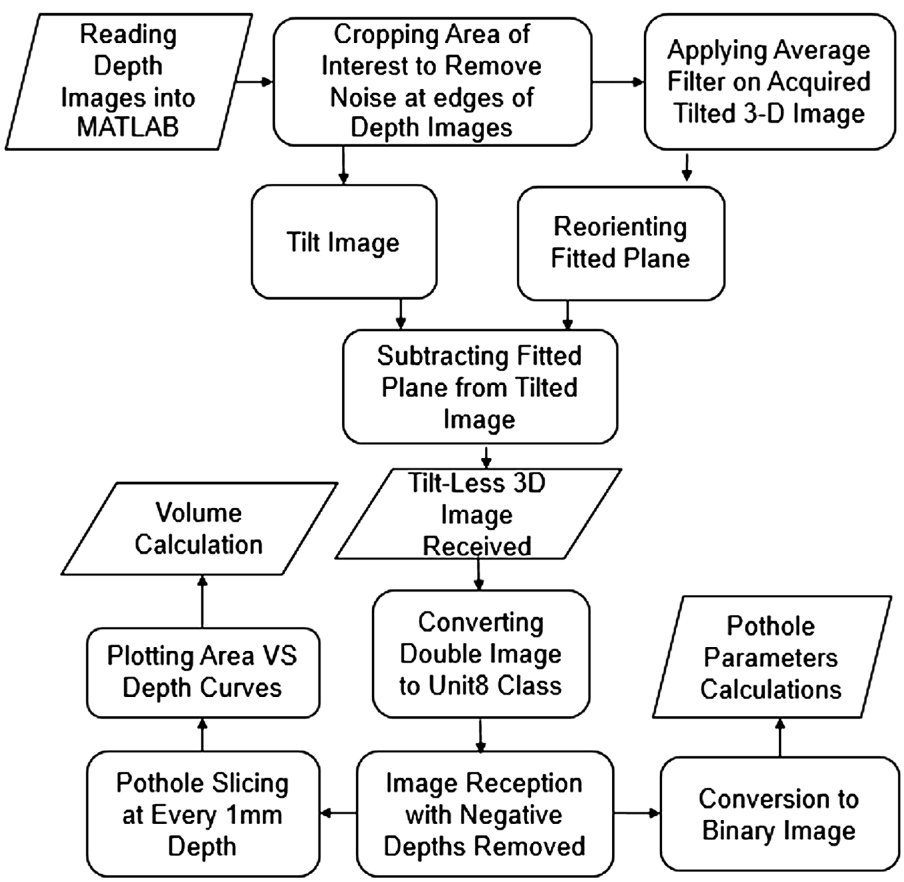

Figure 3. Algorithm flow chart.

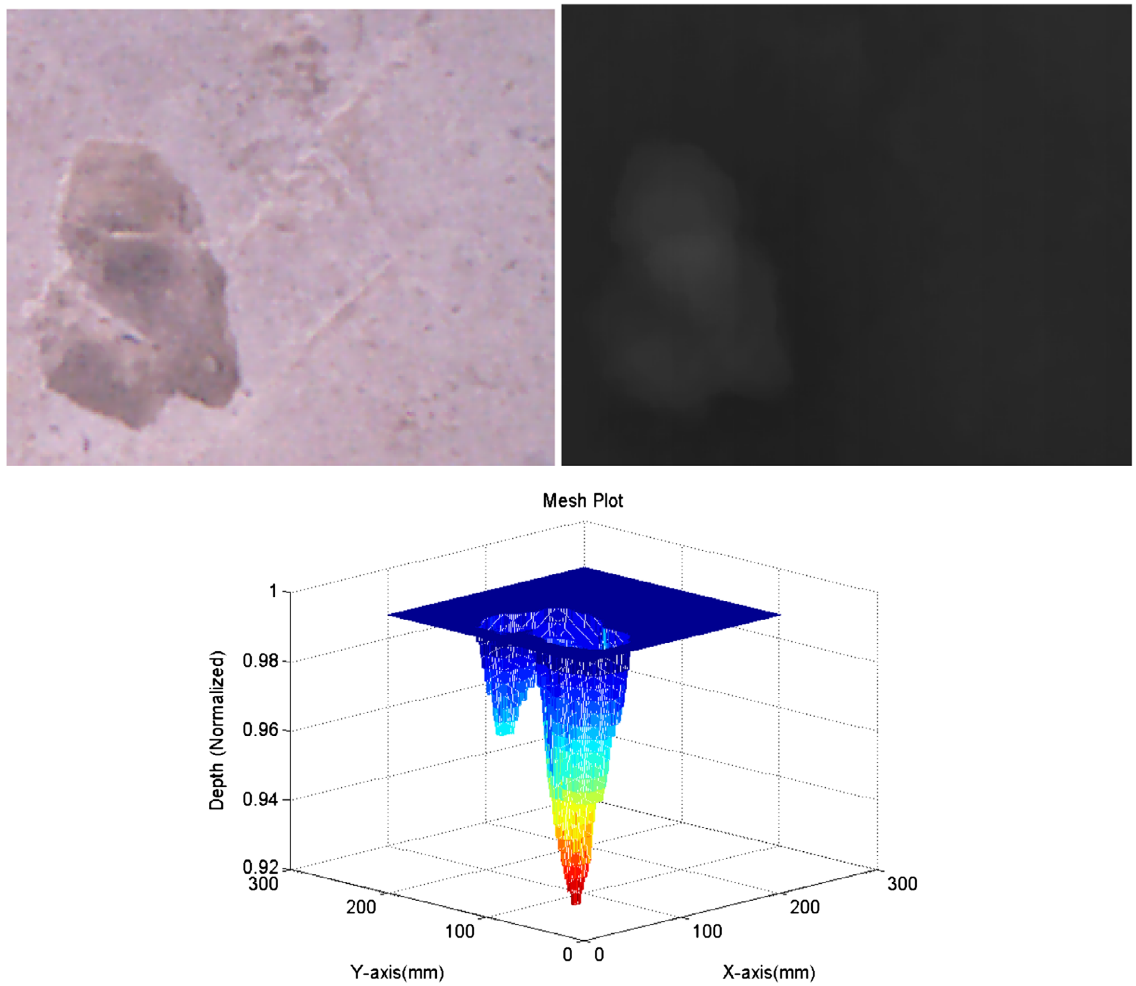

Figure 4. RGB, depth and mesh plot of a natural pothole.

case of pothole length, width and depth. Table 1 highlights the comparison of strengths and limitations of different techniques that are in practice for pothole imaging.

4. Experimental set-up

For analysis and evaluation, imaging is done using the Kinect sensor at NUST College of EME, Rawalpindi, Pakistan in evenings in order to maintain sufficient lighting conditions. The sensor is held at a height of 0.8 m from ground to ensure the minimum working range. As Kinect sensor performance is affected under direct sunlight, therefore, precautions must be taken and a canopy must be placed over the sensor in order to minimise the interference from direct sunlight. The depth images were taken at a resolution of 640 × 480 pixels. The experimental setup is shown in Figure 1. In order to acquire images, the OpenKinect library is used under the Ubuntu operating system. The depth images were analysed further in Matlab.

Figure 2 shows a depth image (left) as well as the corresponding RGB image (right) of a pothole, taken by the Kinect sensor. A depth image or depth map is simply a 2D array of pixels, and each pixel location (x, y) stores depth values in millimetres that are sensed by the IR sensor. Higher values represent surface points that are far away from the sensor.

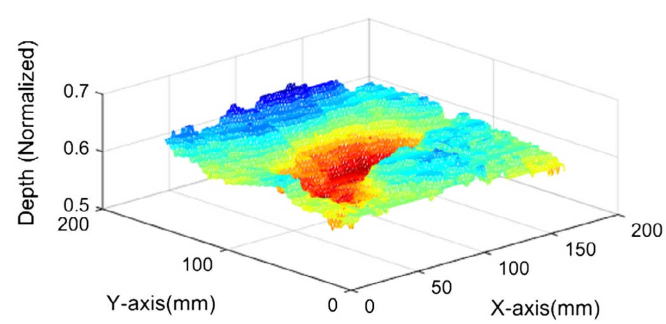

Figure 5. Mesh plots of potholes.

As mentioned earlier that the depth or the z-axis value is already in real-world coordinate system (mm); whereas, x and y coordinates are represented as pixel locations. Therefore, the x-axis and the y-axis are converted to the real-world coordinate system (mm) using Kinect depth and its field of view through Equations (1) and (2) (Elsbree 2012).

$$W_x = n_x \times d \times \alpha \tag{1}$$

$$W_y = n_y \times d \times \beta \tag{2}$$

Table 2. Pothole feature table.

Pothole	Length (mm)			Width (mm)			Perimeter (mm)			Max depth (mm)		
	Calculated	Measured	%Error	Calculated	Measured	%Error	Calculated	Measured	%Error	Calculated	Measured	%Error
a	548.1	602	9.0	234.9	287	18.1	2715	3050	11.0	39	34	14.7
b	222.9	215	3.7	200.0	181	10.5	1161	1036	12.1	52	47	10.6
c	240.5	220	9.3	99.2	120	17.3	879.1	720	22.1	37	34	8.8
d	290.9	330	11.8	209.6	260	19.4	1537	1390	10.6	33	31	6.5
e	893.4	1040	14.1	651.2	770	15.4	4942	4130	19.7	48	50	4.0
f	622.8	660	5.6	343.5	380	9.6	3355	2930	14.5	40	37	8.1
g	790.4	700	12.9	480.5	420	14.4	9354	7893	18.5	39	35	11.4
h	729.9	650	12.3	376.5	450	16.3	3122	2539	22.9	49	48	2.1
MPE			9.8			15.1			16.4			8.3

Table 3. Additional metrological features.

Pothole	Centroid (mm, mm)	Eccentricity	Orientation (degree)	Volume (cm^3)
a	255.00, 177.00	0.9035	41.89	3071.29
b	218.00, 233.00	0.4419	56.22	1799.76
c	106.00, 172.00	0.9109	−36.10	673.89
d	190.00, 185.00	0.6934	34.93	921.07
e	255.00, 170.00	0.6847	−0.71	14,979.38
f	255.00, 199.00	0.8341	−8.90	5456.94
g	255.00,187.00	0.7940	−6.30	5913.80
h	255.00, 174.00	0.8567	−4.69	8859.94

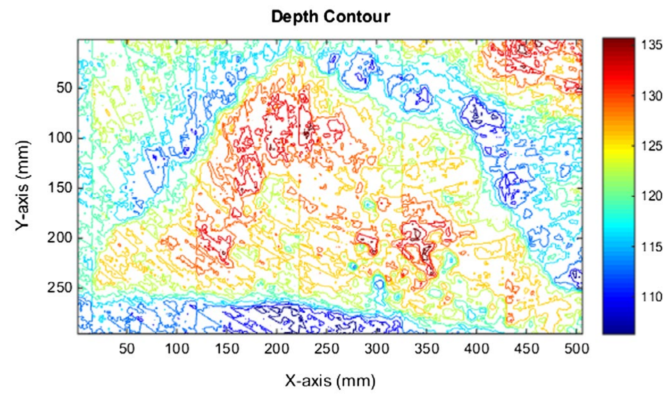

Figure 6. Contour plot of pothole.

where, W_x is the world coordinate in x direction, n_x is the normalised coordinate values along x-axis ranging from 0 to 1, d is the depth in mm, α is the constant based on Kinect's field of view for x-axis = 1.12032, W_y is the world coordinates in y direction, n_y is the normalised coordinate values along y-axis ranging from 0 to 1, and β is the constant based on Kinect's field of view for y-axis = 0.84024.

5. Algorithm

This section describes the data processing algorithm that is developed in order to process and extract the metrological as well as characteristic features of potholes. The metric depth images are captured using Openkinect library under Ubuntu Linux environment. Subsequently these images are imported in Matlab and are read as gray scale images ranging from 0 to 2^{16} using Matlab uint16 (16 bit unsigned integer) class. These images show variation in intensity of gray level from 0 which represents the zero depth and is shown by a black pixel to 2^{16} representing full depth shown by a white pixel. 3D meshes of different potholes with normalised depth are produced for better visualization. The x and y coordinates of these meshes are in real world coordinate system (mm) while the depth values are normalised between 0 and 1. After the images are imported in Matlab, uint16 data type is converted to double data type and meshes of the potholes are generated. This is shown in Figure 4. A slight disorientation in the sensor creates a tilt in the data. This tilt due to disorientation is a source of error, hence, must be removed in order to evaluate pothole parameters correctly. To remove the tilt, a plane is fitted by applying averaging filter to the depth image. The averaging filter is given by Equation (3):

$$g(x, y) = \frac{\sum_{s=-a}^{a} \sum_{t=-b}^{b} w(s, t) f(x+s, y+t)}{\sum_{s=-a}^{a} \sum_{t=-b}^{b} w(s, t)} \tag{3}$$

Here, $f(x, y)$ is the input image, $w(s, t)$ is the averaging mask of size $m \times n$ pixels, whereas $a = (m-1)/2, b = (n-1)/2$.

The fitted plane is then subtracted from the tilted image to remove the tilt. The corrected image is then processed to get different parameters like major axis, minor axis and volume, of the pothole. For volume calculation, the algorithm first performs thresholding of the grayscale depth image to binarised it. The pothole appears white in the binarised image. Thresholding is done by the Otsu method, and depth images are binarised for every millimetre of depth. For each step, number of white pixels in the binary images is calculated. Area at a certain depth is calculated by multiplying number of white pixels at that depth level to the area of one pixel in real-world coordinates. The area at each depth level is summed the trapezoidal rule given by Equation (4):

$$\int_a^b f(x)\mathrm{d}x \approx \frac{h}{2} \sum_{k=1}^{N} \left(f(x_{k+1}) + f(x_k) \right) \tag{4}$$

where a and b are the lower and upper limits, h is the grid spacing and is given by $h = (b-a)/2$ and N is the total number of equally spaced intervals.

The algorithm takes approximately 4 s on Intel core i3 processor to produce results. Figure 3 shows flowchart of the developed algorithm.

6. Results

About 70 experiments are performed for 30 surveyed potholes of different shapes and sizes. Figure 4 shows the mesh plot of a pothole, produced by the algorithm. The RGB and depth images of the pothole are shown as well.

Similarly, Figure 5 shows the mesh plots of a pothole. As it can be seen from the figure that the dark blue region is closer to the road surface and the dark red region depicts the maximum depth level of the pothole. Regions in the other colours show depth values in between the two extremes and are multiple of 2^{16}. Table 2 summarises metrological parameters of the different surveyed potholes.

Table 2 provides important metrological features of different potholes such as, length, width, perimeter and maximum depth against their actual values, whereas Table 3 presents some

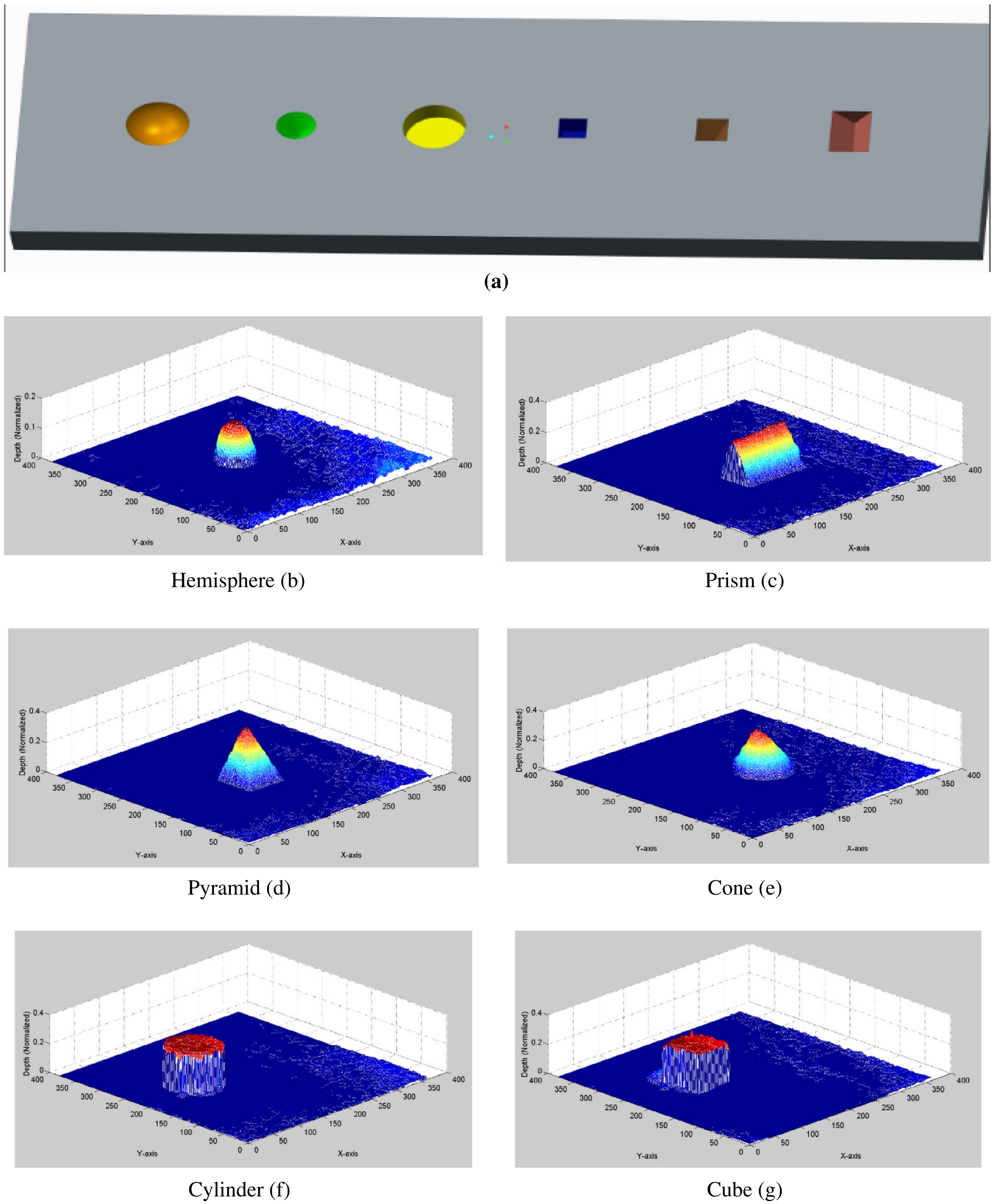

Figure 7. CAD model (a) and mesh plots of artificially created potholes (b)–(g).

Table 4. Pothole maximum depth and volume table.

Pothole	Maximum depth (mm)			Volume (cm^3)		
	Actual	Calculated	Error (%)	Actual	Calculated	Error (%)
Hemisphere	40	41	2.5	150	144	4.0
Prism	78	81	3.8	545	582	6.8
Pyramid	100	97	3.0	340	320	5.9
Cone	81	82	1.2	403	433	7.4
Cylinder	80	82	2.5	950	875	7.9
Cube	78	80	2.5	780	773	0.8
		MPE = 2.58%			MPE = 5.47%	

Figure 8. Pothole filled with water.

additional meteorological features of potholes that are calculated through proposed algorithm.

Length and width provide an idea of the geometrical feature of the potholes. Centroid provides us the information regarding the geometrical centre of pothole. The eccentricity provides the information regarding the shape of the pothole. For a perfectly circular geometry, the value of eccentricity should be zero; however, it can be said that potholes with eccentricity values closer to zero are circular, whereas for potholes having eccentricity values closer to 1 are longitudinal or elliptical in shape. Information related to pothole shape may be used to judge the severity of deterioration. For example, a shallow, but wide, pothole does not introduce extreme levels of stresses to the surrounding area. On the contrary, a narrow, deep pothole results in a stress concentration around it, leading to further degradation. Orientation provides the measure of tilt of the major axis of pothole in degrees with respect to x-axis ranging from −90 to 90. Figure 6 shows the contour plot of a pothole.

7. Benchmarking and performance analysis

For benchmarking purposes a test-rig is developed with standard shapes of known dimensions to calculate error in measurements of the sensor that is the more practical way for benchmarking (Gonzalez-Jorge *et al.* 2013). A concrete test-rig containing six artificial potholes of different shapes and dimensions is developed. Figure 7 shows the CAD model of the test-rig, it also shows the mesh plots of the artificially created potholes by the proposed algorithm.

Table 4 shows the percentage error in the volume and depth measurements, 30 experiments are performed in this regard. The mean percentage error (MPE) in depth calculations is found to be 2.58 and 5.47% for the depth and volumetric calculations, respectively.

Under rainy weather, potholes are often filled with water as shown in Figure 8; therefore, imaging is not possible using conventional imaging equipment. However, as Kinect uses infrared technology, therefore, analysis is done to evaluate sensor performance using potholes filled with water.

As under rainy conditions, water is usually mixed with mud and sometimes with leaked lube oil of the cars; therefore, the performance of the sensor is analysed not only with the clear water, but also with the muddy and the oily water.

7.1. *Performance under clear water*

Experimentation is done to evaluate Kinect's performance in the case, where potholes are filled with water at different volume levels. The artificial potholes in the test-rig are filled with water at 20, 60 and 100% of their volume and results are calculated. The results are presented in Table 5. A reduction in the volumetric measurements is observed with gradual increase in water quantity. Mesh plots of a cylindrical pothole at different water levels are shown in Figure 9. It is clear from the figure that there is considerable reduction in depth measurement; however, no abrupt change is observed. Though some amount of infrared is absorbed in water but it can be concluded that performance of sensor is still be able to measure depth and this is not possible at all with techniques like stereo-vision.

7.2. *Performance under muddy water*

Another experiment is done to assess the performance of the sensor in the case, where potholes are filled with muddy water

Table 5. Measurements of pothole filled with clear water.

Pothole name	Actual volume	20% filled		60% filled		100% filled	
		Mean	Error (%)	Mean	Error (%)	Mean	Error (%)
Prism	545	566	4	516	5	453	17
Pyramid	340	304	10	298	12	290	14
Cone	403	297	26	262	34	258	36
Cylinder	950	877	8	816	14	710	25
Cube	780	610	21	557	28	574	26

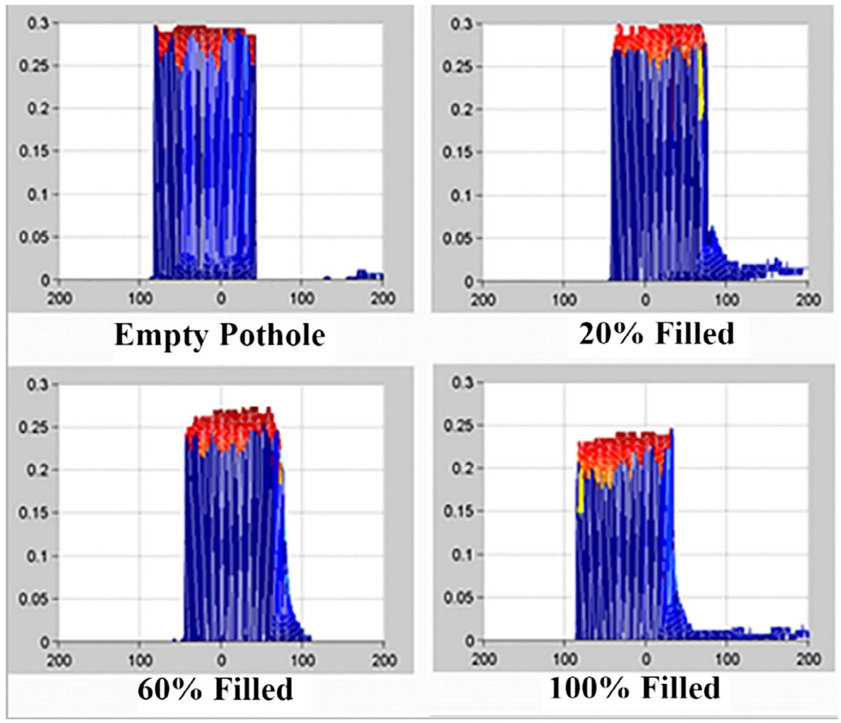

Figure 9. Meshes showing pothole filled with different content of water.

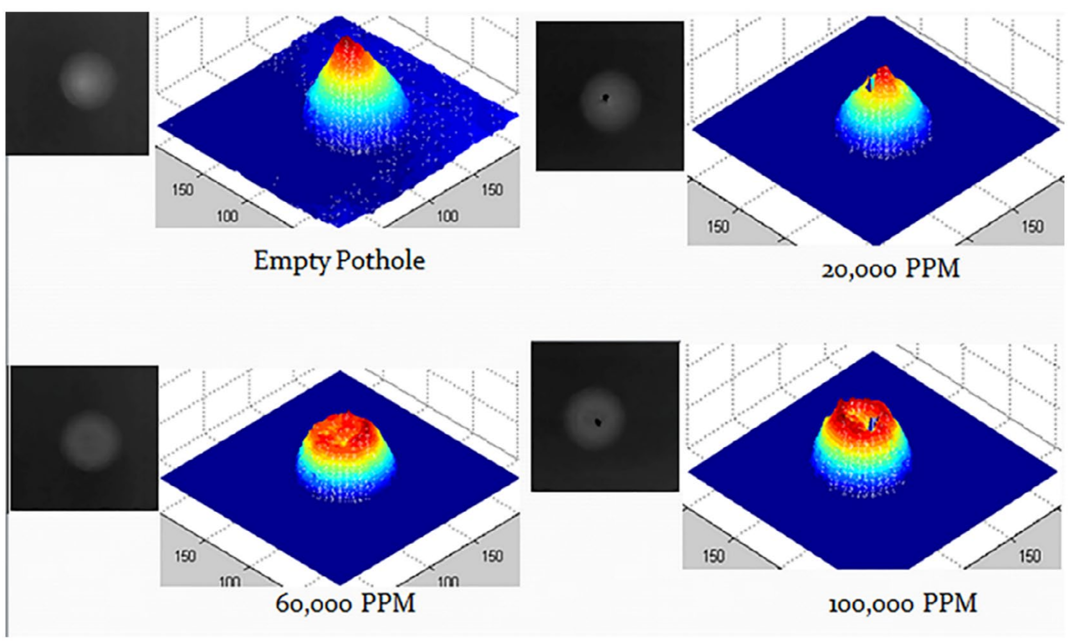

Figure 10. Pothole meshes at different PPM of dust in water.

Table 6. Measurements of pothole filled with muddy water.

		20,000 PPM		60,000 PPM		100,000 PPM	
Pothole name	Actual volume	Mean	Error (%)	Mean	Error (%)	Mean	Error (%)
Prism	545	507	6	197	63	149	72
Pyramid	340	177	47	116	65	108	68
Cone	403	161	60	162	66	185	54
Cylinder	950	798	16	773	18	731	23
Cube	780	653	16	662	15	579	26

at different concentrations. The test-rig potholes are filled with 100 ml of solution with different dust concentrations and mesh plots are generated. Table 6 shows the Kinect measurements at different parts per million (PPM) of dust present in the water. A random behaviour in measurements is observed due to random distribution of suspended dust particles. The mesh results are shown in Figure 10. Under muddy conditions where infrared reflects back from surface of muddy water considering it an opaque surface. Also, due to suspended dust particles, sometimes the infrared from the sensor lose its strength and does not make its way back to the sensor. In this case, the sensor is unable to find any depth value, providing zero depth at a particular location and a random error is introduced in calculations. These two types of errors are the main cause of randomness in error values.

7.3. Performance under oily water

Experimental results are obtained for potholes filled with a mixture of lube oil and water in order to study the sensor response at different lube oil concentrations in a 100-ml solution. The test-rig potholes are filled with 100 ml of solution at lube oil concentration of 0.5, 1, 1.5, 2 and 2.5 ml and measurements are obtained. The results are presented in Table 7. A random behaviour in results is observed due to random distribution of undissolved lube oil on the surface of water. The results are shown in Figure 11. However, the measurements made by Kinect sensor are not affected by lube oil spillage on the pavement surface itself.

7.4. Error introduced due to surface roughness

Kinect sensor works on structured light principle in which a known pattern of IR beam is projected through IR projector onto an object or a surface, and inferring depth from the distortion in the pattern being received by the IR sensor. This distortion in the pattern is due to any change or variation in the surface profile and is taken as a depth value. The depth map of the surface is created by the built-in algorithm of the Kinect sensor.

Surface roughness is defined as an irregularity in the pavement surface. Therefore, this irregularity introduces error in the measurements made by the sensor. To detect the noise introduced by surface roughness in measurements, the algorithm first binarises the depth images at every 1 mm of depth level and detects roughness as a group of few white pixels that are not actually connected to the pothole region. This surface roughness eventually disappears with increasing depth of the pothole.

Binary images of an artificial pothole at different depth levels are shown in Figure 12. It can be seen from the figure that the fourth binary image (the right most image in the first row) depicts depth level at initial 10 mm. At this level, the pothole boundary is less affected by the surface roughness of the

Table 7. Measurements of pothole filled with oily water.

Pothole name	Actual volume	0.5 ml		1 ml		1.5 ml		2 ml		2.5 ml	
		Mean	Error (%)	Mean	Error (%)	Mean	Error (%)	Mean	Error (%)	Mean	Error (%)
Prism	545	402	26	136	75	159	70	214	60	238	56
Pyramid	340	141	58	19	94	46	75	63	81	68	80
Cone	403	180	55	26	93	171	57	64	84	72	47
Cylinder	950	738	22	522	45	650	31	191	79	60	93
Cube	780	639	18	554	28	444	43	44	94	7	99

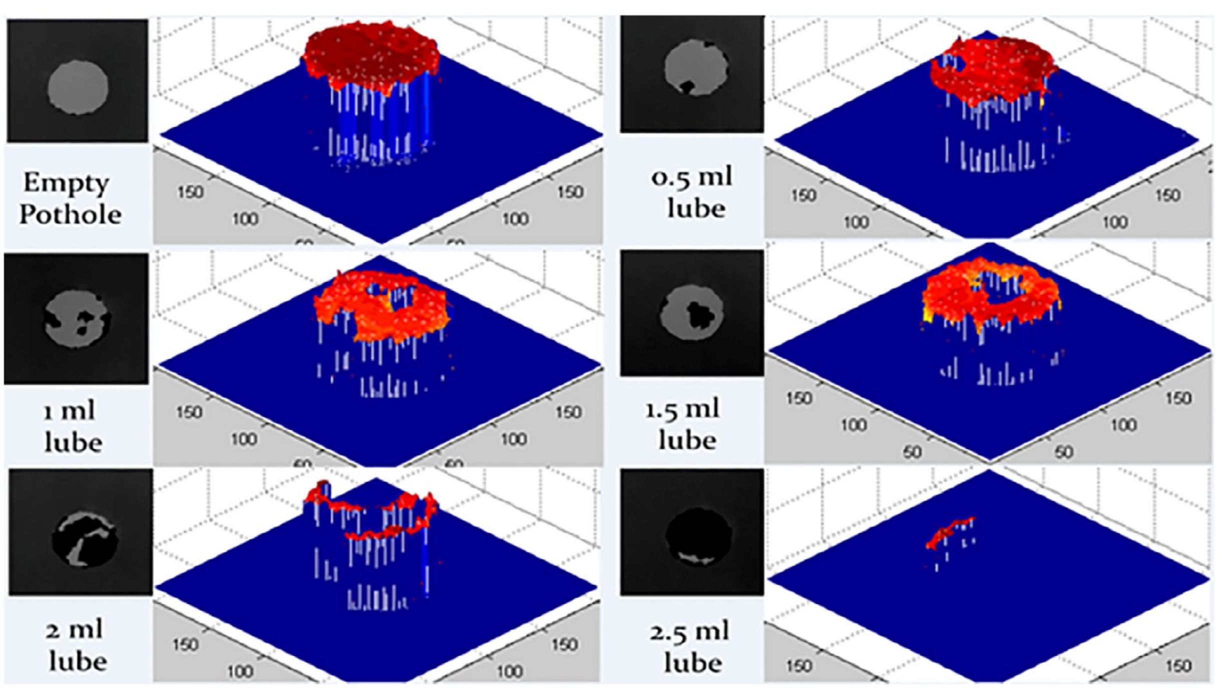

Figure 11. Pothole meshes at different content of lube oil on the surface of water.

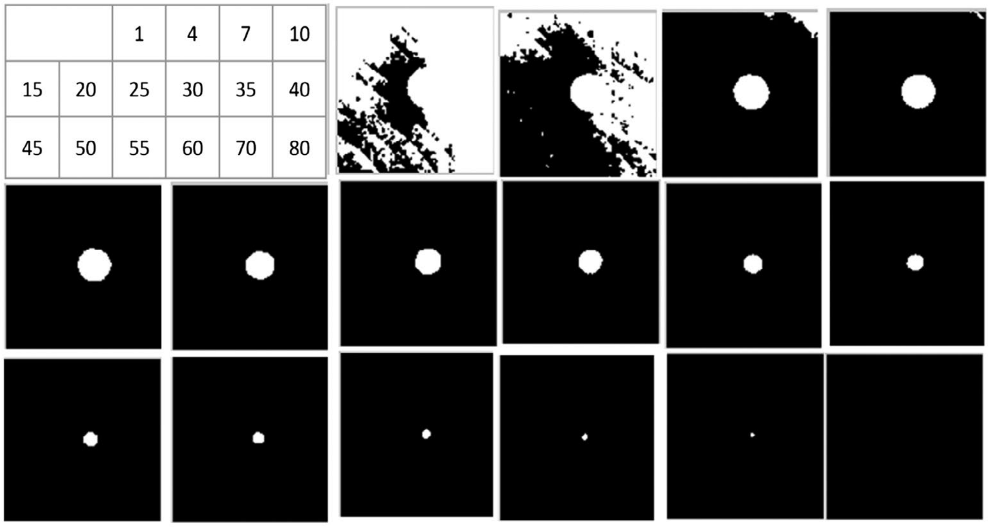

Figure 12. Binary images of circular indentation at depths of 1, 4, 7, 10, 15, 20, 25, 30, 35, 40, 45, 50, 55, 60, 70 and 80 mm.

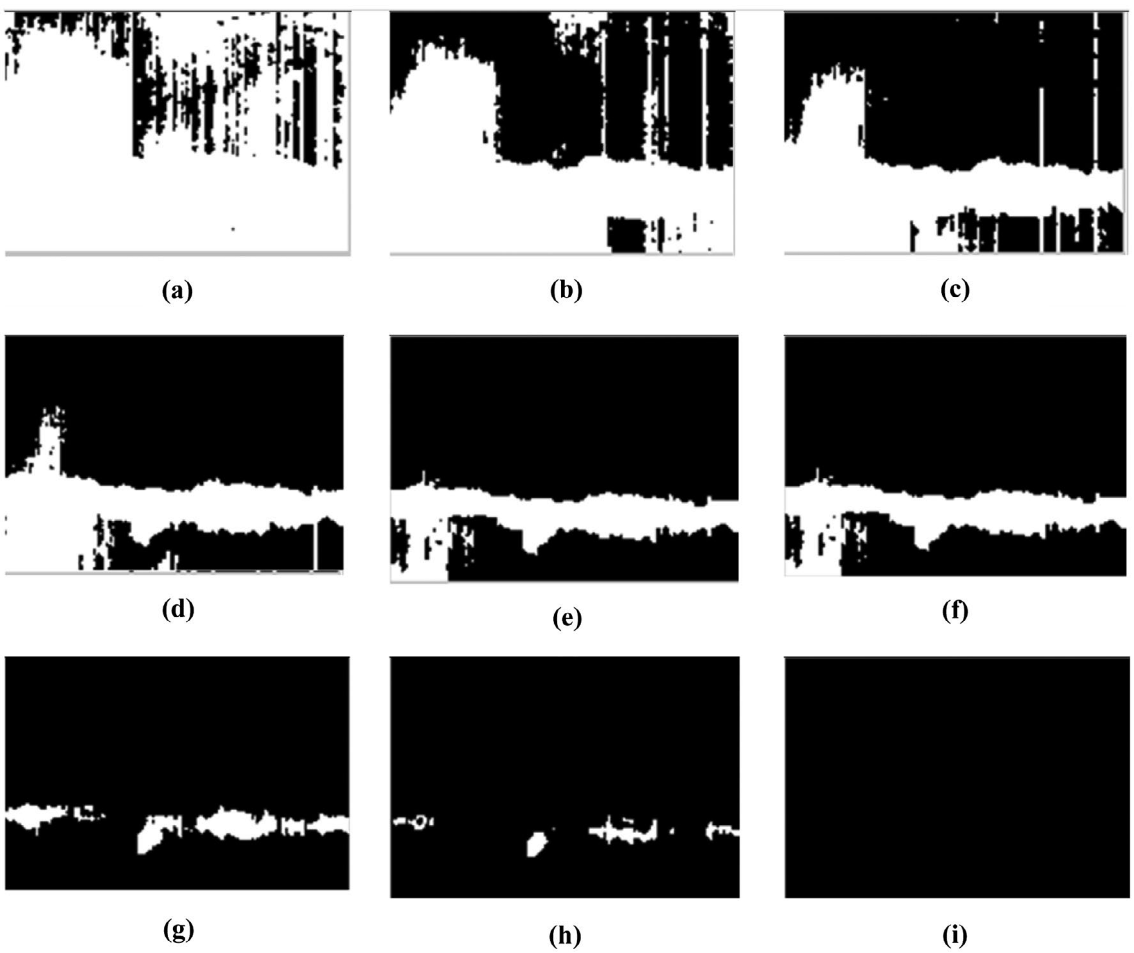

Figure 13. Binary images of an actual pothole at depths of 1, 4, 7, 10, 13,16,19,22 and 25 mm.

pavement as compared to the images at depth levels 1, 4 and 7 mm (the images left to 10 mm image) that are highly affected. The image at depth level of 15 mm does not have any effect of surface roughness. Therefore, error due to surface roughness should be adjusted between 10 and 15 mm of depth by taking the average of all the depth measurements made by the sensor between 10 and 15 mm. However, this roughness may vary for different surfaces, therefore, should be adjusted accordingly. The algorithm adjusts this by replacing the affected data points with average of all depth measurements for detected range of noise.

This holds the same for a natural pothole of irregular shape as shown in Figure 13.

7.5. Errors due to negative depth

Positive texture (i.e. 'negative depth' in terms of the convention used in this work) is observed due to pebbles, stones, etc. on the road surface, which if not adjusted by the algorithm, will become a root cause for errors in metrological calculations. After plane fitting, negative depths appear as negative data values. It is compensated by converting *double* data class of Matlab to the *uint8* (8 bit unsigned integer) class, therefore, removing the negative depths by converting each negative value to zero.

8. Discussion

This work presents a method whereby a cost-effective sensor from is used as a potential scanner for potholes. The following are the key contributions of this paper, when compared to the available literature on using Kinect for pothole metrology.

(1) A benchmarking process with well-defined samples of various shapes, in order to evaluate the performance of the sensor.
(2) The RANSAC method, used in (Joubert *et al.* 2011, Jahanshahi *et al.* 2012), is avoided for plane fitting as it is found to have poor repeatability (Hast and Marchetti 2012). An average value-based method is used in this work.
(3) Camber of the road surface is taken into account, before correcting for it. This approach is required as the central part and the sides of a given pavement are oriented in different directions, owing to the natural, curved shape of a road. Hence, without a tilt correction, potholes in different parts of the road will get subjective treatments from the algorithm.
(4) When compared to Jahanshahi *et al.* (2012), who used the rectangle method for volume calculations, this paper uses the trapezoidal method.
(5) The paper, in comparison to the others, pay special attention to the non-ideal situations often encountered when imaging roads, by the way of water build up and water being contaminated by other materials, such as oil spills.

9. Conclusions

The Kinect sensor shows considerable results for the visualisation and metrological analysis of the potholes. Different metrological and geometrical parameters of the potholes are extracted by analysing the depth images acquired by the sensor. The depth images provide more detailed information regarding pavement distress as compared to 2D vision. When compared to laser triangulation techniques, the proposed technique with Kinect is much cheaper. The sensor is shown to be suitable for finding the geometric parameters of potholes, such as major axis, minor axis, centroid, eccentricity, orientation, perimeter, maximum depth and volume. Results show MPE of 2.58 and 5.47% in depth and volumetric calculations, respectively for artificial potholes of known dimensions. The sensor measurements are affected under water accumulation, where potholes are filled with water. A decrease in volume calculation is observed as the water content in pothole in increased. Results with muddy water show the limitation of Kinect sensor in finding volume. Under muddy conditions where infrared reflects back from the surface of muddy water considering it an opaque surface. In the case of suspended dust particles, the sensor is unable to determine the depth value, providing zero depth at a particular location and a random error is introduced in calculations. When lube oil is spilled on road surface then the sensor is able to find depth information efficiently but the lube oil film on surface of water in potholes create a worst case scenario where infrared loses its strength and the depth cannot be measured by the sensor at those specific areas, thus, introducing a large error in measurements. Hence, it can be concluded that under normal conditions the sensor can be utilised for pavement inspection with considerable accuracy.

Disclosure statement

No potential conflict of interest was reported by the authors.

References

Aksamit, P. and Szmechta, M., 2011. Distributed, mobile, social system for road surface defects detection. *In*: *5th international symposium on computational intelligence and intelligent informatics (ISCIII), 2011*, 15–17 September Floriana USA, 37–40.

Bianchini, A., Bandini, P., and Smith, D., 2010. Interrater reliability of manual pavement distress evaluations. *Journal of Transportation Engineering*, 136 (2), 165–172.

Correa, D.S.O., *et al.*, 2012. Mobile robots navigation in indoor environments using kinect sensor. *In: 2012 Second Brazilian Conference on Critical Embedded Systems (CBSEC)*, IEEE, 36–41.

Cruz, L., Lucio, D., and Velho, L., 2012. Kinect and RGBD images: challenges and applications. *In*: *2012 25th SIBGRAPI conference on graphics, patterns and images tutorials (SIBGRAPI-T)*, 22–25 August Ouro Preto, 36–49.

El-laithy, R. A., Huang, J., and Yeh, M. 2012. Study on the use of Microsoft Kinect for robotics applications. *In: Position Location and Navigation Symposium (PLANS)*, Myrtle Beach, South Carolina, USA, 1280–1288.

Elsbree, J. 2012. Available from: http://qa.social.msdn.com/Forums/en-US/kinectsdknuiapi/thread/e53a4ba7-2522-407f-9d60-86e6fc5f89dc [Accessed November 2014].

Eriksson, J., *et al.*, 2008. The pothole patrol: using a mobile sensor network for road surface monitoring. *In*: *Proceedings of the 6th international conference on mobile systems, applications, and services (MobiSys '08)*. New York: ACM, 29–39.

Gonzalez, W. and Woods, R.E., 2004. *Eddins, digital image processing using MATLAB*. 3rd ed. Upper Saddle River, NJ: Prentice Hall.

Gonzalez-Jorge, H., *et al.*, 2013. Metrological evaluation of Microsoft Kinect and Asus Xtion sensors. *Measurement*, 46 (6), 1800–1806.

Hast, A. and Marchetti, A. 2012. Putative match analysis: a repeatable alternative to RANSAC for matching of aerial images. *In*: *International conference on computer vision theory and applications, VISAPP2012*, 24–26 February, Rome, Italy. 341–344.

Jahanshahi, M.R., *et al.*, 2012. Unsupervised approach for autonomous pavement-defect detection and quantification using an inexpensive depth sensor. *Journal of Computing in Civil Engineering*, 27 (6), 743–754.

Jin, L. and Yayu, L., 2010. Potholes detection based on SVM in the pavement distress image. *In*: *Ninth international symposium on distributed computing and applications to business engineering and science (DCABES), 2010*, August Hong Kong, 544–547.

Jog, G.M., *et al.*, 2012. Pothole properties measurement through visual 2D recognition and 3D reconstruction. *In: Proceedings of the ASCE*

International Conference on Computing in Civil Engineering, Clearwater Beach, FL, 553–560.

Joubert, D., *et al.*, 2011. Pothole tagging system. *In*: *4th robotics and mechatronics conference of South Africa (RobMech 2011)*. 23–25 November. Pretoria: CSIR International Conference Centre.

Koch, C. and Brilakis, I., 2011. Improving pothole recognition through vision tracking for automated pavement assessment. *In*: *Proceedings of the 18th EG-ICE workshop on intelligent computing in engineering*, 6–8 July, Twente, Netherlands. 1–8.

Laurent, J., Talbot, M., and Doucet, M., 1997. Road surface inspection using laser scanners adapted for the high precision 3D measurements of large flat surfaces. *In*: *Proceedings. International conference on recent advances in 3-D digital imaging and modeling, 1997.*, 12–15 May, Ottawa, 303–310.

Liu, J.X., 2006. *Computer vision and robotics*. New York, NY: Nova.

Moazzam, I., *et al.*, 2013. Metrology and visualization of potholes using the Kinect sensor. *In*: *16th international IEEE conference on intelligent transportation systems – (ITSC), 2013*, October, The Hague, 1284–1291.

Picche, A., 2013. How potholes are eating city budgets. Available from: http://www.cbsnews.com/news/how-potholes-are-eating-city-budgets/ [Accessed April 2014].

Rakprayoon, P., Ruchanurucks, M., and Coundoul, A. 2011. Kinect-based obstacle detection for manipulator. *In: 2011 IEEE/SICE International Symposium on System Integration (SII)*, IEEE, 68–73.

Rajab, M.I., Alawi, M.H., and Saif, M.A., 2008. Application of image processing to measure road distresses. *WSEAS Transactions on Information Science & Applications*, 5 (2008), 1–7.

Salari, E. and Bao, G., 2011. Automated pavement distress inspection based on 2D and 3D information. *In*: *IEEE international conference on electro/information technology (EIT), 2011*, 15–17 May Mankato, MN, 1–4.

Salari, E. and Yu, X., 2011. Pavement distress detection and classification using a genetic algorithm. *In*: *Applied imagery pattern recognition workshop (AIPR), 2011 IEEE*, October. 1–5, Washington, DC, 1–5

Wang, K.C. and Gong, W., 2002. Automated pavement distress survey: a review and a new direction. *In*: *Pavement evaluation conference, 2002*, Roanoke, VA, USA.

Asphalt Industry Alliance, 2014. *Annual local authority road maintenance (ALARM) survey*. Available from: http://www.asphaltindustryalliance.com/ [Accessed April 2014].

Yao, X., Yao, M., and Xu, B., 2008. Automated detection and identification of area-based distress in concrete pavements. *In*: *7th international conference on managing pavement assets*. Calgary Alberta, Canada.

Youquan, H., *et al.*, 2011. A research of pavement potholes detection based on three-dimensional projection transformation. *In*: *4th international congress on image and signal processing (CISP), 2011*, Vol. 4, 15–17 October. 1805–1808.

Yu, X. and Salari, E., 2011. Pavement pothole detection and severity measurement using laser imaging. *In*: *IEEE international conference on electro/information technology (EIT), 2011*, 15–17 May Mankato, MN, 1–5.